EasyChair Preprint

№ 15848

A Pilot Study Examines the Experimentally and Numerical Analysis of an AGMD Membrane Distillation System

Mokhless Boukhriss, M Ali Maatoug, Timoumi Mahdi,
El Ouni Nizar, Mansouri Sami and Jammeli Adel

February 20, 2025

A pilot study examines the experimentally and numerical analysis of an AGMD membrane distillation system

Mokhless. Boukhriss[1,2*], M Ali Maatoug[2], Mahdi.Timoumi[2], Nizar el ouni [2,] Sami.Mansouri[2], Adel Jammeli[2]

Abstract— ***This study presents findings from an innovative membrane distillation system, effectively integrated with a sustainable solar water heater, designed to produce high-quality potable water with minimal saline discharge, regardless of the source water's salinity. The research focuses on optimizing and experimentally analyzing air gap membrane distillation (AGMD) within a pilot plant setup. Results reveal that permeate flux increases with higher feed temperature and flow rate, while reducing the air gap by 5 mm further improves efficiency. A one-dimensional model, based on established transfer equations and correlations, was used to evaluate the pilot system, achieving a peak permeate flux of 4 kg/m²•h at a feed temperature of 80°C and a 1 mm air gap. These results highlight the potential of leveraging low-temperature heat sources for solar desalination projects.***

***Keywords*: Desalination, Membrane distillation, AGMD, solar energy, coupling.**

I. INTRODUCTION

With a global populace anticipated to increase from 7.5 billion in 2017 to 9.6 billion by 2050, the necessity for fresh water keeps escalating, especially considering its daily usage across agriculture, industry, and residential domains [1]. This necessity is particularly pressing in arid regions of Africa and the Near East, where shortages of drinking water are most severe. The process of desalting seawater and brackish sources has surfaced as a feasible answer to generate fresh water. Among the various desalination techniques, membrane distillation (MD) stands out for its capability to function in conjunction with solar energy, which is the chief focus of this investigation [2].

MD is a thermally driven method where water vapor moves through a hydrophobic porous membrane. Within MD, there are four primary module arrangements [3, 4, 5, 6]: direct contact membrane distillation (DCMD), air gap membrane distillation (AGMD), sweeping gas membrane distillation, and vacuum membrane distillation (VMD). This investigation centers on AGMD, selected for its minimal membrane wetting tendency and no extra energy required. The process utilizes a partial pressure difference induced by a temperature gradient across the membrane to facilitate the transport of water vapor. Recent progress in AGMD has been propelled by enhancements in membrane production, bolstering its application in research and practical use. This paper showcases both experimental and simulated findings from a parametric analysis of a pilot-scale PTFE-based AGMD system (500 L), with a modeling emphasis on mass and heat transfer phenomena. The pilot setup is illustrated in Figure 1 (a-b).

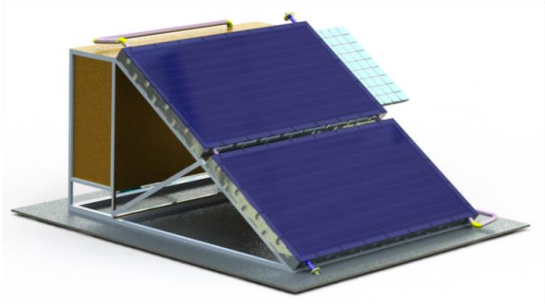

Figure.1-a: Diagram of the proposed facility

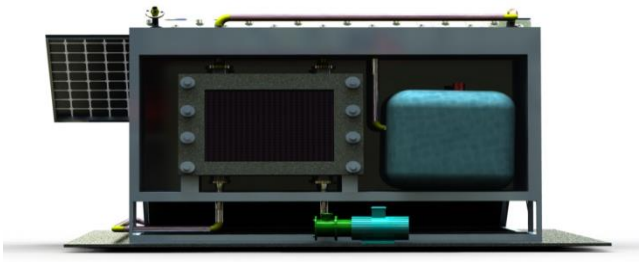

Figure.1-b: rear view

2. Different desalination techniques

Figure 2 categorizes desalination techniques into two main types: membrane processes and thermal processes. These methods impact either the phase state or the chemical bonds in water. Through this approach, saline water is separated into concentrated brine and fresh water with minimal dissolved salts. Although energy-intensive, various desalination methods have been adopted over time, tailored to available energy sources [5].

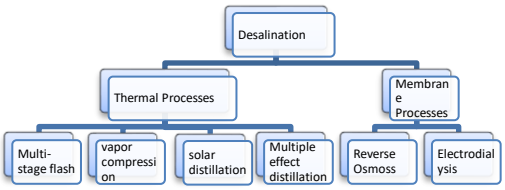

Figure.2: Processes of desalination

2.1. Principles of MD

Water vapor transitions through a hydrophobic porous barrier during the thermal process of Membrane Distillation (MD). The liquid that requires treatment must be in contact with one side of the membrane without penetrating the pores until the pressure across the membrane exceeds the pressure at the inlet. Due to surface tension, the hydrophobic nature of the membrane prevents the liquid from infiltrating the pores, resulting in the formation of interfaces between the liquid and vapor near the pores.

2.2. Various MD Configurations

Configurations of Membrane Distillation in Desalination figure.3.

• Direct Contact Membrane Distillation (DCMD): The membranes are directly exposed to both the feed and permeate sides [16].

• Air Gap Membrane Distillation (AGMD): A layer of air interposes between the membrane and the condensation surface, enhancing energy efficiency but leading to reduced permeate flux.

• Sweeping Gas Membrane Distillation (SGMD): An inert gas on the permeate side removes vapor from the membrane, which subsequently condenses outside.

• Vacuum Membrane Distillation (VMD): A vacuum is applied on the permeate side to boost vapor transfer, making it suitable for treating high-salinity waters and certain chemical separations [17].

Water vapor is transferred via a hydrophobic porous membrane during the thermal process of MD. Until the transmembrane pressure is higher than the inlet pressure, the liquid phase that needs to be treated must remain in contact with one membrane

MD configuration has advantages and limitations based on factors such as energy efficiency, equipment complexity, and permeate flux, making them suited for different desalination and purification applications.

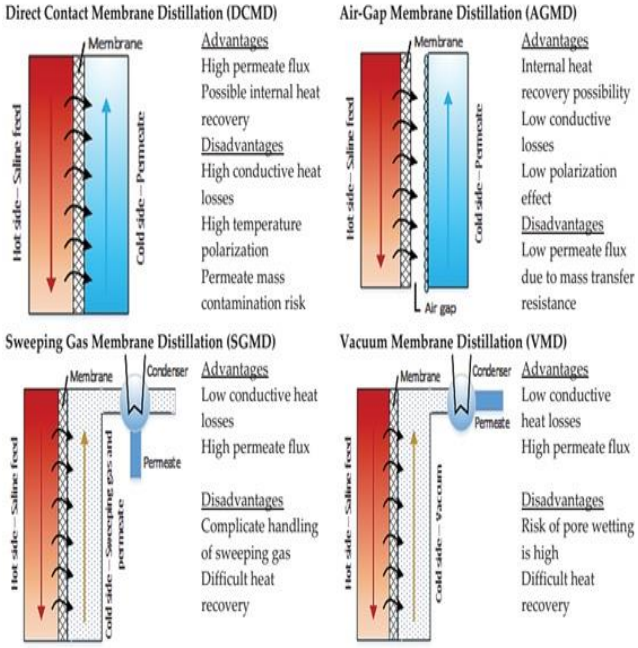

Figure.3: Different configurations of MD

3. The membrane distillation unit's model

The AGMD (Air Gap Membrane Distillation) model depicted in Figure 4 features an intuitive interface to simplify the construction of membrane modules and the generation of numerical solutions. This one-dimensional framework dissects each AGMD element, linking them through pertinent equations to replicate the unit's performance. Properties of the components are articulated via equations [4, 5, 10, 11] found in Table 1, which address the effects of heat transfer, mass transfer, vapor pressure gradients, and thermal conductivity. This approach facilitates swift modifications to system parameters and improves the understanding of AGMD processes.

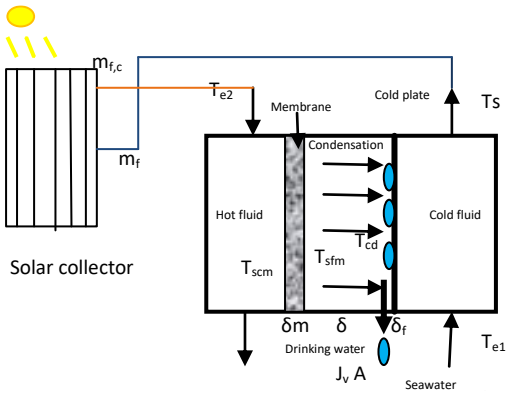

Figure.4: The membrane distillation unit (AGMD) is integrated with a solar collector in this system.

The system employs AGMD modules, and the specifications for the module sizes are detailed in Table 1.

Table .1: lists of membrane parameters and solar collector

Membrane module	
Membrane area (m^2)	12
Width (m)	1.30
Length (m)	0.8
Thickness (mm)	0.14
Pore diameter (mm)	0.22
Porosity	0.78
Tortuosity	1.92
Thermal conductivity (W/m K)	0.175
Hot liquid channel thickness (mm)	0.785
Cold liquid channel thickness (mm)	0.785
Air gap channel thickness (mm)	0.44
Metal foil thickness (mm)	0.985
Thermal conductivity (W/m K)	398

The unfolded screen is shown in figure.5

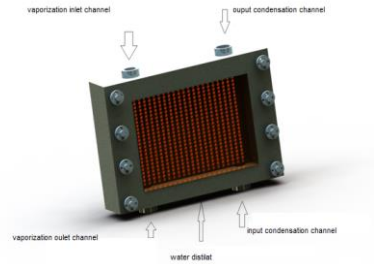

Figure.5: AGMD model

The mathematical model for Air Gap Membrane Distillation (AGMD) focuses on flat-sheet membranes found in commercial MD pilot systems [4-5-8]. The air gap between the membrane and condensation surface minimizes heat loss while allowing vapor transport. The Cooling Plate Sheet absorbs heat from condensate, maintaining essential temperature gradients for vapor transport. This model breaks down heat and mass transfer dynamics within each zone to assess the AGMD unit's efficiency under various conditions [7-9]. The schematic diagram in Figure 6 describes AGMD longitudinal zones with assumptions like constant fluid flow direction, pressure, and thin film condensation [12]. Solar radiation, component designs, integration, business models, and control strategies impact system performance. The model platform enables analysis and control system design. Mass transfer resistance is shifted to the hollow fiber module, considering mass transfer resistance in the gap and membrane while overall heat transfer resistance is evaluated.

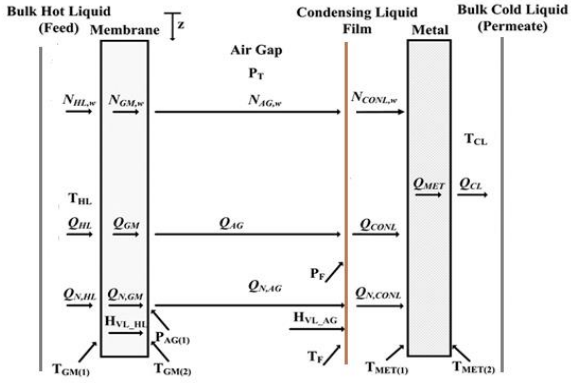

Figure.6: AGMD model for mass and heat transfer

The mass balances

$$\frac{dm_{f,HL}}{dz} = -N_{GM,w} L_w M_w \quad (1)$$

$$\frac{dm_{f,CONL}}{dz} = -N_{AG,w} L_{MD} M_w \quad (2)$$

$$N_{GM,w} = N_{AG,w} \quad (3)$$

Balancing the energy

$$\frac{\partial T_{HL}}{\partial t} = -W_{MD}\left[\frac{m_{f,HL}}{M_{HL}}\frac{\partial T_{HL}}{\partial z} + \frac{L_{MD}}{M_{HL}C_{p,HL}}\left(h_{HL} + N_{GM,w}C^{L}_{p,w}M_w\right)\left(T_{GM(1)} - T_{GM(2)}\right)\right] \quad (4)$$

$$\frac{\partial T_{cL}}{\partial t} = -W_{MD}\left[\frac{m_{f,CL}}{M_{CL}}\frac{\partial T_{CL}}{\partial z} + \frac{L_{MD}h_{CL}}{M_{CL}C_{p,CL}}\left(T_{MET(2)} - T_{CL}\right)\right] \quad (5)$$

$$Q_{HL} + Q_{N,HL} - H_{VL,HL} = Q_{GM} + Q_{N,GM} \quad (6)$$

$$Q_{GM} + Q_{N,GM} = Q_{AG} + Q_{N,AG} \quad (7)$$

$$Q_{AG} + Q_{N,AG} + H_{VL,AG} = Q_{CONL} + Q_{N,CONL} \quad (8)$$

$$Q_{MET} = Q_{CONL} + Q_{N,CONL} \quad (9)$$

$$Q_{MET} = Q_{CL} \quad (10)$$

Mass fluxes

$$N_{GM,W} = \frac{k_{GM,w}}{RT_{GM,arg}}\left(P^{sat}_{GM(1),w} - P^{sat}_{AG(1),w}\right) \quad (11)$$

$$N_{AG,W} = \frac{k_{GM,w}}{RTarg P_{In,air}\ \delta_{AG}}\left(P^{sat}_{AG(1),w} - P^{sat}_{F,w}\right) \quad (12)$$

Heat fluxes

$$Q_{HL} = h_{HL}\left(T_{HL} - T_{GM(1)}\right) \quad (13)$$

$$Q_{GM} = [\varepsilon h_{GM} + (1+\varepsilon)h_{MEM}](T_{GM(1)} - T_{GM(2)}) \quad (14)$$

$$Q_{AG} + Q_{N,AG} = h_{AG}\frac{\theta}{e^{-\theta}}\left(T_{GM(2)} - T_F\right) \quad \text{Avec}$$

θ=NCp/h (15)

$$Q_{CONLL} = h_{CONL}\left(T_F - T_{MET(1)}\right) \quad (16)$$

$$Q_{MET} = h_{MET}\left(T_{MET(1)} - T_{MET(2)}\right) \quad (17)$$

$$Q_{CL} = h_{CL}\left(T_{MET(2)} - T_{CL}\right) \quad (18)$$

$$Q_{N,HL} = N_{GM,N}C^{L}_{p,w}\left(T_{HL} - T_{GM(1)}\right) \quad (19)$$

$$Q_{N,GM} = N_{GM,N}C^{L}_{p,w}\left(T_{GM(1)} - T_{GM(2)}\right) \quad (20)$$

The relationships identified by Shock and Miquel [15] for the flat plate wound membrane module are utilized to evaluate the heat transfer coefficients for both the hot and cold fluid sides.

$$\mathrm{Nu} = 0.065.\mathrm{Re}^{0.875}.\mathrm{Pr}^{0.25} \quad (24)$$

For the condensing heat transfer to the film, the following relationship is employed: [13]

$$h_{CONL} = 0.943\left[\frac{\rho^{L}_{w}\left(\rho^{L}_{W} - \rho^{V}_{W}\right)g\Delta H_{vap,w}K^{L}_{W}}{L_{MD}\,\mu_w\left(T_{CONL} - T_{MET}\right)}\right] \quad (25)$$

4. Results and discussion

4.1. Membrane distillation unit simulation

4.1.1. Validation of the model under various operating conditions

In these trials, reproducibility was emphasized, maintaining variations in water vapor flux within ±0.12 kg/m².hr (2%), which signifies accurate measurements. The precision of the model was evaluated by juxtaposing its forecasted mass fluxes with observed data across feed water temperatures ranging from 40°C to 80°C. The findings revealed an exponential rise in AGMD flux as feed water temperatures increased, aligning with established trends in AGMD literature [14, 15, 17], thereby affirming the model's capability to capture typical flux dynamics. Although additional refinement is essential to

boost prediction accuracy for particular applications, the model's forecasts closely correlated with empirical data within the bounds of experimental error, establishing a dependable basis for future scaling and sophisticated analyses Figure 7.

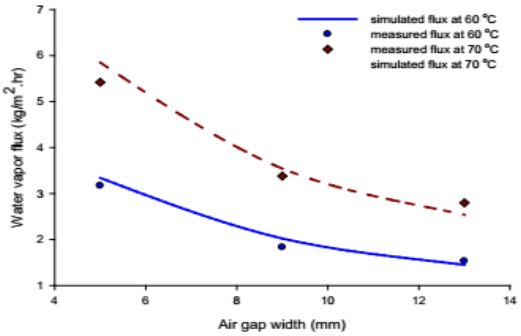

Figure 7: Water vapor fluxes were measured and simulated at various temperatures of the deionized feed water.

We replaced deionized water with Red Sea water (feed) to enhance the validation of the model and to examine its predictions regarding water vapor flux at a seawater salinity of 4.2 weight percent. To identify any possible pore wetting, we continuously monitored the conductivity of the distillate, which consistently stayed below 20 µS. The expected water vapor flux also fell within the range of experimental error, as illustrated in Figure 8.

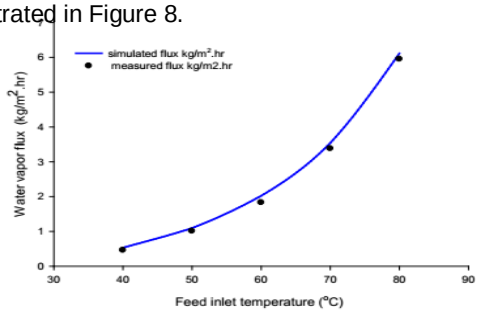

Figure.8: Water vapor fluxes at various seawater feed temperatures were predicted and measured.

In Figure 9, the research investigated the influence of air gap width on flux. The model demonstrated that flux diminishes as air gap width expands, aligning with findings from Kimra et al. [16] and Jonsson et al. [17]. Nevertheless, the predictions related to flux alterations with increasing air gap width were less precise compared to those for variations in feed temperature. The results revealed that water vapor flux exhibits considerable sensitivity to the width of the air gap, particularly when the gap is narrow, as slight measurement inaccuracies (e.g., 0.1 mm) can notably impact flux. Measurement inaccuracies were approximately ±0.5 mm, probably due to the deformation of the parafilm tape utilized for sealing. Future experiments with an upgraded module are anticipated to enhance model predictions at small air gaps [18-19].

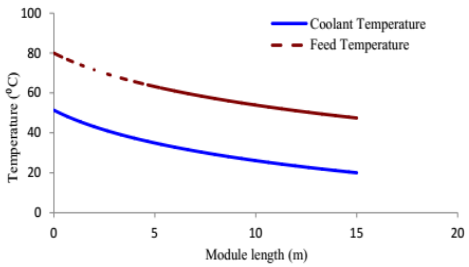

Figure.9: Water vapor fluxes predicted and measured in relation to air gap

The model underwent validation against experimental results utilizing different membrane pore sizes. Although it failed to accurately forecast the data for the 0.45 µm membrane at a feed temperature of 70 °C, leading to a 15% discrepancy, the overall predictions from the model were deemed satisfactory within a ±10% range (refer to Figure 10). As the feed temperature increases, there is a marked rise in flux, indicating that changes in inlet temperature will exert a more significant influence on the observed flux in this range than at lower feed temperatures. Thus, the 15% discrepancy seems justified

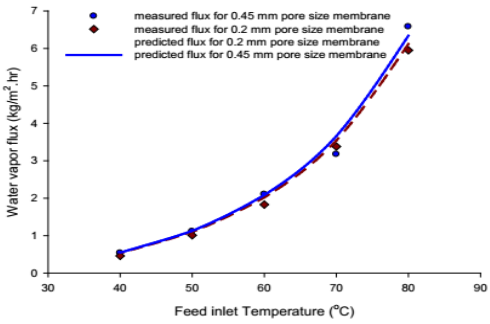

Figure 10: Water vapor fluxes were both predicted and measured across membranes with varying pore sizes..

4.1.2. Influence of the flow regime

The established model can replicate flow rates across the flat membranes in AGMD systems, as shown in Figure 11, which depicts the temperature distributions of the heated feed water and cooling fluid within the module. In a counter-current arrangement, a steady temperature gradient is noted throughout the module, although this may change if the flow rates of the coolant and feed do not match. Mass transfer in membrane distillation (MD) relies on diffusion and is greatly affected by the thickness of the membrane wall and the size of the pores. The investigation verified that the type of membrane affects the efficiency of MD: membranes with larger pore sizes, assuming similar wall thicknesses, achieve superior flux. Both molecular diffusion and Knudsen diffusion play roles in mass transfer, leading to enhanced permeate flux with increased pore diameters [20-21].

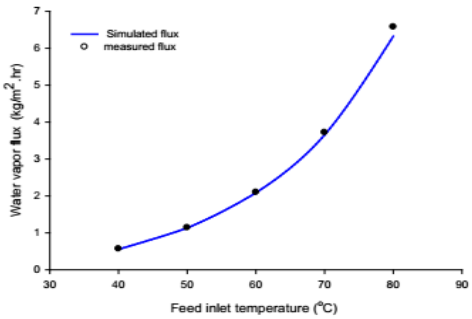

Figure**.11:** demonstrates the effect of feed temperature and membrane classification on thermal performance, where both the feed (mF) and distillate (mD) are maintained at a rate of 0.014 dm³/s, with a feed temperature (TD) set at 20 °C.

5. Conclusions

In this research, the membrane distillation setup was analyzed through both simulations and practical experiments. Pilot-scale experimental findings were employed to create and validate a theoretical framework, which also verified the dimensions of the prototype solar collector linked to the AGMD unit. The focus of the investigation was on three essential parameters: supply temperature, flow rate of the hot fluid, and thickness of the air gap. It was observed that variations in the supply of high-temperature fluid have a lesser effect on flow dynamics compared to variations in flow rate, with this influence diminishing as the air gap thickness increases. A peak permeate flux of 7.4 kg/m²h was attained at a fluid temperature of 80°C, an air gap of 1.04 mm, and a flow rate of 5 l/min for both hot and cold fluids. This research illustrates that demineralized water can be generated by AGMD even at hot water supply temperatures as low as 25°C, indicating its suitability for low-temperature heat sources. The principal obstacles to advancing this desalination technology are the effects of prolonged use and membrane fouling, which will be explored further in forthcoming tests.

Nomenclature

A - Area (m^2)
B - Effective absorptivity
Cp - Heat capacity (J/kg•K)
D - Diffusion coefficient (m^2/s)
Fj - Objective function j
H - Height (m)
HVL - Heat transfer rate caused by phase change ($J/m^2•s$)
h - Heat transfer coefficient ($W/m^2•K$)
I - Intensity of solar irradiation (W/m^2)
K - Thermal conductivity (W/m•K)
Kc - Proportional gain
Ku - Ultimate gain
k - Mass transfer coefficient (m/s)
L - Length (m)
M - Mass (kg)
Mw - Molecular weight of H_2O (kg/kmol)
mf - Fluid flow rate (kg/s)
mf,c - Fluid collector flow rate (kg/s)
N - Mass flux ($kmol/m^2•s$)
OP - Controller output
P - Pressure (Pa)
Q - Heat transfer rate (J/s)
QN - Sensible heat transfer rate (J/s)
R - Gas constant (J/kmol•K)
S - Collector absorber surface area (m^2)
Si - Stream number i
T - Temperature (K)
U - Overall heat transfer coefficient of the heat exchanger ($W/m^2•K$)
U' - Total heat loss coefficient between the collector absorber and environment ($W/m^2•K$)
W - Width (m)
ΔHvap - Heat of vaporization (J/kmol)
d - Thickness (m)
ε - Membrane porosity
μ - Viscosity (kg/m•s)
ρ - Density (kg/m^3)
τ - Membrane tortuosity
τi - Integral time (s)
τu - Ultimate period (s)

Subscripts

L - Liquid
G - Gas
Sat - Saturated
AG - Air gap
A - Ambient
Air - Air
Avg - Average
c - Solar collector
CL - Cold liquid
CONL - Condensate liquid
F - Condensing film surface in air gap
F - Circulating fluid in the solar collector
fh - Circulating fluid between coil and heat exchanger
fs - Circulating fluid between internal coil and solar collector
Tf - Fluid temperature (K)
Tc - Collector temperature (K)
GM - Gas in membrane
HL - Hot liquid
MD - Membrane module
MEM - Membrane
MET - Metal
Nu - Nusselt number
Pr - Prandtl number
Re - Reynolds number
T - Total
w - Water
wa - Water-air

References

[1] Lloyd, D.R., & Lawson, K.W. (1997). Membrane distillation. *Journal of Membrane Science, 124*, 1-25.

[2] Bourawi, M.S., Ding, Z., Ma, R., & Khayet, M. (2006). A framework for better understanding the membrane distillation separation process. *Journal of Membrane Science, 285*, 4-29.

[3] Kalogirou, S.A. (2005). Seawater desalination using renewable energy sources. *Progress in Energy and Combustion Science, 31*, 242-281.

[4] Banat, F., Jwaied, N., Rommel, M., Koschikowski, J., & Wieghaus, M. (2007). Performance evaluation of the "large SMADES" autonomous desalination solar-driven membrane distillation plant in Aqaba, Jordan. *Desalination, 217*, 17-28.

[5] Banat, F., Jwaied, N., Rommel, M., Koschikowski, J., & Wieghaus, M. (2007). Desalination by a "compact SMADES" autonomous solar-powered membrane distillation unit. *Desalination, 217*, 29-37.

[6] van Medevoort, J., Jansen, A., Hanemaaijer, J.H., Dotremont, C., Nelemans, B., van Sonsbeek, E., et al. (2008, November). Memstill: seawater desalination as a solution to water scarcity. Presented at *BMG-NMG Membrane Symposium*, Antwerp, Belgium.

[7] Ben Bacha, H., Bouzguenda, M., Damak, T., Abid, M.S., & Maalej, A.Y. (2000). A study of a water desalination station using the SMCEC technique: production optimization. *Renewable Energy, 21*, 523-536.

[8] Roca, L., Berenguel, M., Yebra, L., & Alarcón, D.C. (2008). Preliminary modeling and control studies in the AQUASOL project. *Desalination, 222*, 466-473.

[9] Aspen Technology, Inc. (2006). Aspen Custom Modeler, Version. Cambridge, MA: Aspen Technology, Inc.

[10] Ben Bacha, H., Damak, T., Bouzguenda, M., Maalej, A.Y., & Ben Dhia, H. (2003). A methodology to design and predict operation of a solar collector for a solar-powered desalination unit using the SMCEC principle. *Desalination, 156*, 305-313.

[11] Avlonitis, S., Hanbury, W.T., & Ben Boudinar, M. (1993). Performance of spiral wound modules: an analytical solution—Part II. *Desalination, 89*, 227-246.

[12] Chang, H., Liau, J.S., Ho, C.D., & Wang, W.H. (Accepted). Simulation of membrane distillation modules for desalination using a user's model on the Aspen Plus platform. *Desalination.*

[13] Holman, J.P. (1989). *Heat Transfer*. New York: McGraw-Hill.

[14] Koschikowski, J., Wieghaus, M., & Rommel, M. (2003). Solar thermal-driven desalination plants based on membrane distillation. Desalination, 156, 295-304.

[15] Schock, G., & Miquel, A. (1987). Mass transfer and pressure loss in spiral wound modules. Desalination, 64, 339-352.

[16] Chen, C.X., Yu, L.X., & Dai, T.Y. (1996). Review of new membrane and membrane process. Technology of Water Treatment, 22(6), 307-313.

[17] Liu, L.Y., Ding, C.W., & Chang, L.J., et al. (2008). Progress in membrane separation enhanced by ultrasound. Chemical Industry and Engineering Progress, 27(4), 32-37.

[18] Mokhless Boukhriss. Sofiene Khemili. Mohamed Bechir Ben Hamida. Habib Ben Bacha. 2018, Simulation and experimental study of an AGMD membrane distillation pilot for the desalination of seawater or brackish water with zero liquid discharged **;** Heat and Mass Transfer · May 2018- DOI: 10.1007/s00231-018-2383-60.

[19] Mokhless Boukhriss ;· Med Bechir Ben Hmida·,Med Ali Maatoug :· Kamel Zarzoum :· Riadh Marzouki Habib Ben Bacha1,2020, The design of a unit sweeping gas membrane distillation: experimental study on a membrane and operating parameters Applied Water Science (2020) 10:110 https://doi.org/10.1007/s13201-020-01194-3.

[20] Boukhriss, M., Zarzoum, K., Maatoug, MA ., & Timoumi, M. (2021). Innovation of Solar Desalination System Coupled with Solar Collector: Experimental Study. Journal of Advanced Research in Fluid Mechanics and Thermal Sciences , 80 (1),94 111.https://doi.org/10.37934/arfmts.80.1.94111

[21] Mokhless Boukhriss**,** Mehdi Timoumi, Habib Ben Bacha, Experimental of membrane distillation unit coupled with a DCMD using solar energy, Solar Compass, Volume 7,2023,100055,ISSN 2772-9400, https://doi.org/10.1016/j.solcom.2023.100055.